

Synthesis of SAPO-34/ZSM-5 Composite and Its Catalytic Performance in the Conversion of Methanol to Hydrocarbons

Liping Li,^{a,b,c} Xiaojing Cui,^a Junfen Li^a and Jianguo Wang^{*,a}

^aState Key Laboratory of Coal Conversion, Institute of Coal Chemistry, Chinese Academy of Sciences, P.O. Box 165, 030001 Taiyuan, Shanxi, PR China

^bCollege of Chemistry and Environmental Engineering, Shanxi Datong University, 037009 Datong, PR China

^cUniversity of Chinese Academy of Sciences, 100049 Beijing, PR China

SAPO-34/ZSM-5 composite was synthesized with nano-sized ZSM-5 zeolite as seeds and characterized by powder X-ray diffraction (XRD), scanning electron microscopy (SEM), nitrogen sorption, Fourier transform infrared (FTIR) and temperature-programmed desorption of ammonia (NH₃-TPD); its catalytic performance in the conversion of methanol to hydrocarbons (MTH) was investigated. The results indicated that the as-synthesized SAPO-34/ZSM-5 composite takes the form of sphere-like particles with a diameter ranging from 2.3 to 4.8 μm, through the accumulation of tiny ZSM-5 and SAPO-34 crystals; a large quantity of mesopores was formed in the interspaces between the ZSM-5 and SAPO-34 crystals. Owing to its proper acidity and porosity, the SAPO-34/ZSM-5 composite exhibits higher stability in MTH and favors the formation of aromatics and alkanes, compared with the parent SAPO-34 and ZSM-5 zeolites and their mechanical mixture.

Keywords: SAPO-34, ZSM-5, composites, methanol-to-hydrocarbons, hydrothermal synthesis

Introduction

As methanol can be expediently produced via syngas from multifarious carbon sources such as coal, natural gas, and biomass, the conversion of methanol to hydrocarbons (MTH) over acidic zeolite catalysts has been turning into an increasingly important alternative to petrochemical processing to get hydrocarbons.^{1,2} Relying on the catalyst and reaction conditions employed, the MTH process may be designed to get light olefins (methanol to light olefins, MTO), gasoline (methanol to gasoline, MTG), aromatics (methanol to aromatics, MTA), and so on.

Usually, the molecular sieves of 8 to 12-membered ring are employed as the catalysts in MTH;³⁻⁶ among them, SAPO-34 and ZSM-5 zeolites have proved to be uniquely effective. SAPO-34 as a catalyst for MTO has been successfully used in commercial plants, with high yield of light olefins.⁷ However, SAPO-34 is apt to deactivation from coke deposition because of its narrow channels; moreover, its phosphorus aluminum framework is hydrothermally less stable than silicon

aluminum molecular sieves. Compared with SAPO-34, on the contrary, ZSM-5 exhibits excellent hydrothermal stability and better resistance to coking in MTH, but lower selectivity to light olefins.

In recent years, the synthesis of composite molecular sieves as well as their application in catalysis has attracted extensive attention. The composite molecular sieves obtained from zeolites with different frameworks may not only possess the intrinsic characteristics of the parent zeolites, but also display a peculiar capability that is deficient for the parent zeolites. For example, Fan *et al.* prepared various composite molecular sieves consisting of SAPO-11, H β , HMOR and HZSM-5;^{8,9} among them, ZSM-5/SAPO-11 composite exhibited a core-shell structure, large quantity of mesopores, moderate acidity, and then excellent catalytic performance in fluid catalytic cracking gasoline hydro-upgrading. In addition, SAPO-11/H β composite with modified acidity showed high catalytic activity in 2-butylene cracking.¹⁰ The catalytic activity of micro/mesoporous β /MCM-41 composites for toluene alkylation with propylene was also greatly enhanced.¹¹ In the alkylation of toluene with dimethyl carbonate, the selectivity to *p*-xylene was greatly improved over the

*e-mail: iccgw@sxicc.ac.cn

H-MCM-22/MCM-41 composite catalyst, owing to the decrease of external Brønsted acid sites.¹²

It is then expected that a composite catalyst of SAPO-34/ZSM-5 may take the advantages of both SAPO-34 and ZSM-5 and performs efficiently in MTH, giving high selectivity to specified products and long lifetime.^{13,14} A SAPO-34/ZSM-5 composite, i.e., submicron-scale agglomerates of SAPO-34 and ZSM-5, was prepared and used as an efficient catalyst in MTO.¹³ Meanwhile, it is well accepted that nano-sized crystal zeolites may show high activity and long lifetime because of the large external surface and short diffusion length.¹⁵

Hence, in this work, a SAPO-34/ZSM-5 composite consisting of nano-sized SAPO-34 and ZSM-5 zeolite crystals was synthesized with nano ZSM-5 zeolite as seeds. The SAPO-34/ZSM-5 composite was characterized by powder X-ray diffraction (XRD), scanning electron microscopy (SEM), nitrogen sorption, Fourier transform infrared (FTIR), and temperature-programmed desorption of ammonia (NH₃-TPD); its catalytic performance in MTH was investigated and compared with that of the mechanical mixture of SAPO-34 and ZSM-5.

Experimental

Synthesis procedures

ZSM-5 zeolite with a Si/Al ratio of 200 was hydrothermally synthesized with tetraethyl orthosilicate (TEOS) as the Si source, aluminum isopropoxide as the Al source, and tetrapropylammonium hydroxide (TPAOH) as the template according to the composition of 6 TPAOH:0.1 NaOH:25 SiO₂:0.0625 Al₂O₃:480 H₂O:100 EtOH. All the reagents were obtained from Sinopharm Chemical Reagent Co., Ltd. The crystallization was conducted at 80 °C under static state for 6 days.

SAPO-34 zeolite was hydrothermally synthesized with the synthesis gels prepared from aluminum isopropoxide, orthophosphoric acid (85%, Tianjin chemical reagent factory), fumed silica, tetraethylammonium hydroxide (TEAOH, 35%, Sigma-Aldrich) and water according to the composition of 2 TEAOH:0.3 SiO₂:1 Al₂O₃:1 P₂O₅:100 H₂O. The crystallization was carried out at 170 °C under continuous stirring for 3 days.

SAPO-34/ZSM-5 composite was synthesized by employing the ZSM-5 zeolite as seeds. An appropriate amount of ZSM-5 seeds (in protonic form) was added to the synthesis precursor of SAPO-34. The resultant gel was crystallized at 170 °C under continuous stirring for 3 days. Two sets of SAPO-34/ZSM-5 composite with a weight ratio of SAPO-34 to HZSM-5 being 1 and

1/2 were obtained, which are denoted as C-1 and C-2, respectively.

All the solid products were separated by centrifugation, washed with distilled water for several times, and dried at 100 °C overnight, followed by calcination at 550 °C for 10 h to remove the organic template. To obtain the protonic form ZSM-5, the as-synthesized sample was further treated with 1.0 mol L⁻¹ NH₄NO₃ solution, by refluxing twice at 85 °C for 5 h, and then calcined at 540 °C for 6 h.

For comparison, a mechanical mixture of SAPO-34 and ZSM-5 (denoted as MM) was prepared with an equivalent weight of HZSM-5 and SAPO-34 zeolites.

Characterization

XRD patterns of the as-synthesized samples were recorded at a Rigaku, MiniFlex II desktop X-ray diffractometer using a Cu K α radiation (30 kV, 15 mA), in 2 θ range of 5–40° with a scanning speed of 4° min⁻¹, to identify the crystalline phase.

SEM images of the as-synthesized samples were obtained on a JEM-2010 scanning electron microscopy. High resolution transmission electron microscopy (TEM) measurements were performed on a JEM-2010 transmission electron microscope.

Nitrogen adsorption-desorption isotherms of the calcined samples were obtained on a BELSORP-max instrument at -196 °C. The specific surface area was calculated by the Brunauer-Emmett-Teller (BET) method on the basis of the nitrogen adsorption data in the p/p^0 range corresponding to the linear region of the BET plot. The total pore volume was estimated with the amount of nitrogen adsorbed at the $p/p^0 = 0.99$. The microporous volume and external surface area were calculated by the t-plot method. The micropore surface area was taken as the difference between the total and external surface areas, whereas mesopore volume was the difference between the total and micro pore volumes. The samples were evacuated at 300 °C for 8 h under high vacuum prior to the adsorption measurement.

Infrared (IR) spectra of the calcined samples, which were pressed into a thin wafer with KBr, were acquired in a transmittance mode on a BRUKER TENSOR 27 FTIR spectrometer.

The acidic properties of zeolite samples were determined by NH₃-TPD on an Autochem II 2920 equipment (Micromeritics, USA). Typically, 0.2 g zeolite sample was loaded into a U-type quartz tube reactor and pretreated in helium atmosphere at 600 °C for 30 min. After cooling down to 120 °C, the sample was exposed to a flow of NH₃ for 30 min. After that, the system was purged with helium

at 120 °C for 30 min to remove the physisorbed NH_3 . The NH_3 -TPD profile was then recorded with a thermal conductivity detector (TCD) at temperatures from 120 to 600 °C at a heating rate of 10 °C min^{-1} .

Catalytic tests

The reaction of methanol to hydrocarbons (MTH) was conducted in a fixed-bed micro-reactor under atmospheric pressure at 450 °C, with a weight hourly space velocity (WHSV) for methanol of 1 h^{-1} . High purity nitrogen was used as a diluent gas and the molar fraction of methanol in the feed was 0.2. The gaseous reaction products were analyzed by an on-line gas chromatograph (GC 2014C) equipped with a flame ionization detector (FID) and an Al_2O_3 column and a polyethylene glycol column. The liquid products in aqueous and oil phases were measured by two off-line gas chromatographs (Agilent 7890, FID), the former with an Agilent 19091N-136 column and the latter with an Agilent 19091S-00 column.

Results and Discussion

Structure of the SAPO-34/ZSM-5 composite

Figure 1 presents the XRD patterns of the as-synthesized SAPO-34/ZSM-5 composites (C-1 and C-2), together with those of SAPO-34, ZSM-5, and their mechanical mixture (MM). The XRD pattern of MM is a simple superposition of those for the parent ZSM-5 and SAPO-34, in terms of the peak position and strength of the diffraction peaks. Although the SAPO-34/ZSM-5 composites show all characteristic diffraction peaks of individual ZSM-5 and SAPO-34, their diffraction patterns are distinctly different from that of the mechanical mixture. The diffraction peaks of C-1 and especially C-2 at 2θ of 20.6° and 30.6° for SAPO-34 are obviously widened, suggesting a much smaller crystallite size of SAPO-34 in the SAPO-34/ZSM-5 composites. This may be ascribed to that the addition of ZSM-5 seeds in the precursor leads to a fast formation of crystal nuclei during the synthesis of the composite zeolites. The characteristic peaks for ZSM-5 are stronger in the XRD pattern of C-2 than that of C-1, as more ZSM-5 seeds are introduced to synthesize C-2. In addition, there is a slight shift of diffraction peaks towards lower angle for the SAPO-34/ZSM-5 composites with respect to the parent ZSM-5 and SAPO-34 zeolites, which is not observed for the mechanical mixture, suggesting that there exists an interface interaction between ZSM-5 and SAPO-34 in the composites.

IR spectra of the calcined zeolite samples in the range of 400–1400 cm^{-1} are shown in Figure 2. For ZSM-5, the bands

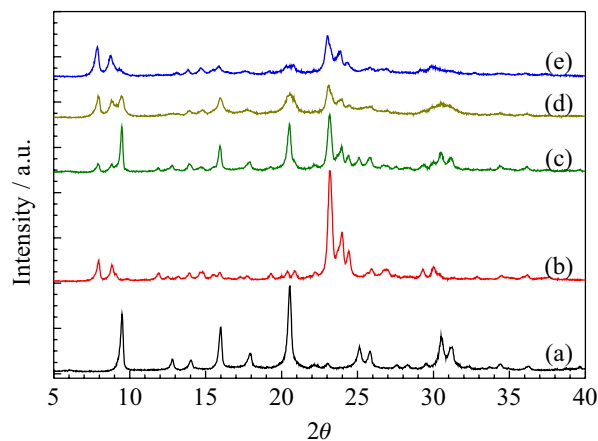


Figure 1. XRD patterns of various zeolite samples: (a) SAPO-34; (b) ZSM-5; (c) SAPO-34 and ZSM-5 MM; (d) SAPO-34/ZSM-5 composite C-1; and (e) SAPO-34/ZSM-5 composite C-2.

at 1100, 800 and 450 cm^{-1} were assigned to the internal vibrations of SiO_4 and AlO_4 , whereas the bands near 550 and 1220 cm^{-1} were ascribed to the double-rings vibration and the asymmetric stretching of SiO_4 and AlO_4 in the zeolite framework, respectively.¹⁶ For SAPO-34, the band at 1200–1000 cm^{-1} was assigned to the asymmetric stretch of T-O tetrahedra, whereas the bands at 740, 640 and around 500 cm^{-1} were corresponding to the symmetric stretch of T-O tetrahedra, the vibration of double 6-membered rings and the bending of T-O, respectively.¹⁷ The MM and composites (C-1 and C-2) exhibit all the characteristic IR bands of the parent SAPO-34 and ZSM-5; however, the bands near 1100 cm^{-1} for the SAPO-34/ZSM-5 composites are shifted towards lower wavenumbers. These results further prove the interface interaction between SAPO-34 and ZSM-5 crystals in the composite, consistent with the XRD results.

Figure 3 shows the SEM images of the as-synthesized SAPO-34/ZSM-5 composites (C-1 and C-2), together

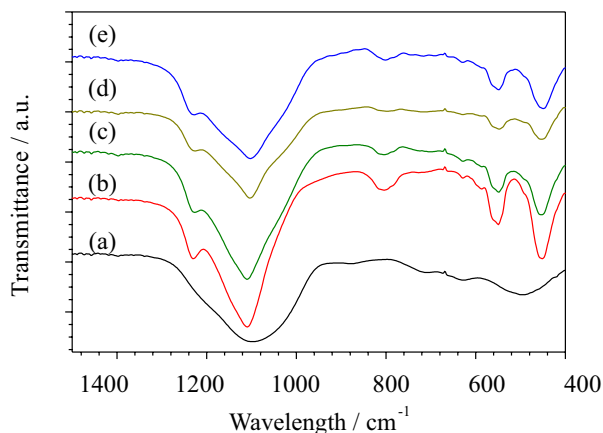


Figure 2. IR spectra of various zeolite samples: (a) SAPO-34; (b) ZSM-5; (c) SAPO-34 and ZSM-5 MM; (d) SAPO-34/ZSM-5 composite C-1; and (e) SAPO-34/ZSM-5 composite C-2.

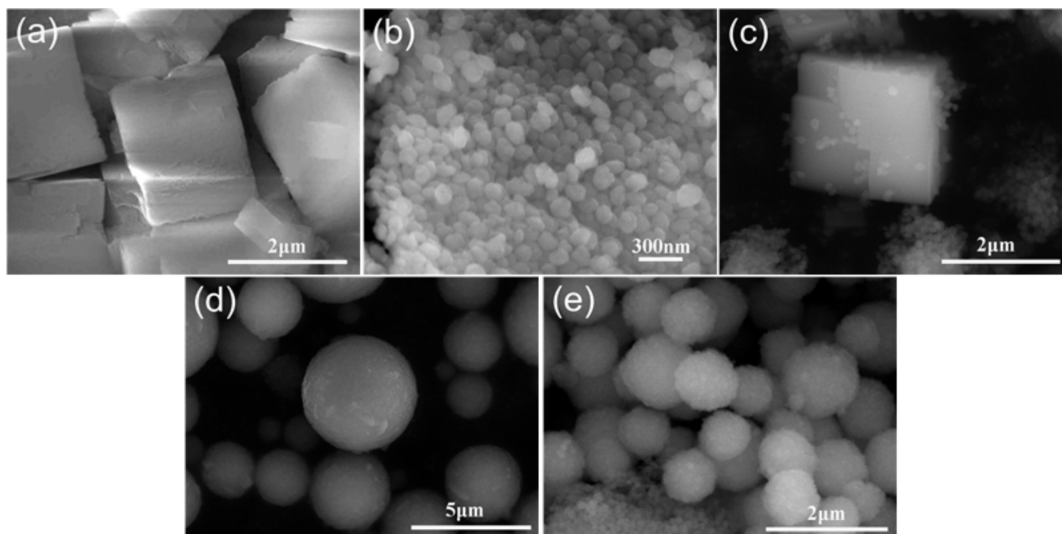


Figure 3. SEM images of various zeolite samples: (a) SAPO-34; (b) ZSM-5; (c) SAPO-34 and ZSM-5 MM; (d) SAPO-34/ZSM-5 composite C-1; and (e) SAPO-34/ZSM-5 composite C-2.

with those of SAPO-34, ZSM-5, and their MM. The parent SAPO-34 and ZSM-5 zeolites exhibit a typical cubic morphology with a crystal size of about 2 μm (Figure 3a) and a ellipse-like nano-crystalline particles of about 100 nm in diameter (Figure 3b), respectively. For the MM, the morphologies of both SAPO-34 and ZSM-5 are observed (Figure 3c). However, the SAPO-34/ZSM-5 composites display a quite different morphology, compared with the parent zeolites, as shown in Figures 3d and 3e. The composite with a SAPO-34/ZSM-5 weight ratio of 1 (C-1) takes the form of sphere-like particles with a diameter ranging from 2.3 to 4.8 μm (Figure 3d). By increasing the amount of ZSM-5 seeds in the synthesis precursor, the sphere-like crystals of the C-2 composite (with a SAPO-34/ZSM-5 weight ratio of 1/2) becomes smaller and the sphere size distribution is more uniform (Figure 3e), compared with that of C-1. Meanwhile, some small crystalline particles of surplus ZSM-5 seeds can also be observed in C-2 (Figure 3e). The sphere-like SAPO-34/ZSM-5 composites seems to be formed through the accumulation of small crystalline particles of SAPO-34 and ZSM-5.

An energy disperse spectroscopy (EDS) analysis was then performed for the microspheres of C-1 and C-2 composites and the distribution of the various elements is illustrated in Figure 4. The well-proportioned changes in the P, Si and Al contents in two composites along with the scanning points suggest that all the elements are uniformly distributed in the composite microspheres. Compared with C-1, C-2 has a higher content of Si, which is relevant to the higher amount of ZSM-5 seeds in the synthesis precursor. The TEM images of the SAPO-34/ZSM-5 composite (C-1) shown in Figure 5 further confirmed that the composite

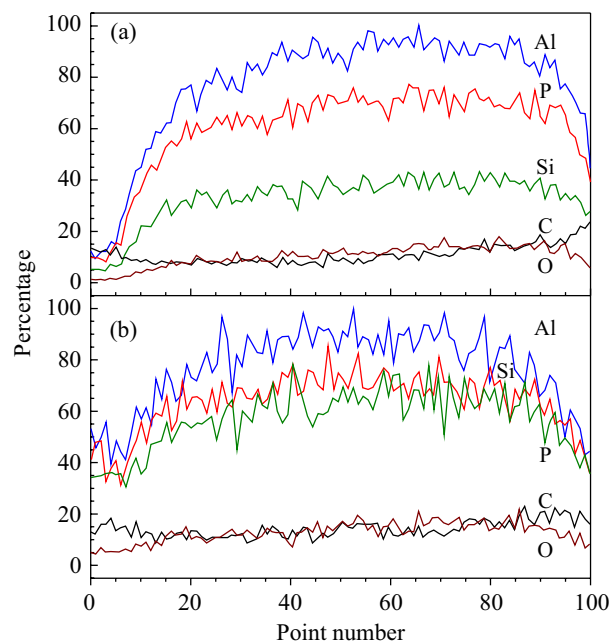


Figure 4. Surface element distribution of the SAPO-34/ZSM-5 composite microspheres: (a) C-1, with a SAPO-34/ZSM-5 weight ratio of 1; and (b) C-2, with a SAPO-34/ZSM-5 weight ratio of 1/2.

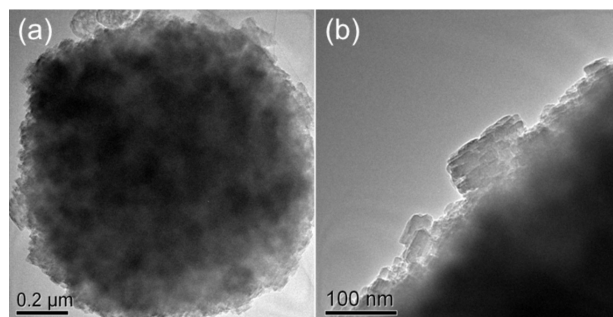


Figure 5. TEM images of the SAPO-34/ZSM-5 composite C-1 (with a SAPO-34/ZSM-5 weight ratio of 1) with different magnifications.

microspheres is formed as a homogeneous aggregation of small SAPO-34 and ZSM-5 crystallites.

Textural properties

The nitrogen adsorption-desorption isotherms of the as-synthesized zeolite samples are displayed in Figure 6 and their textural properties derived are summarized in Table 1. SAPO-34 exhibits a type I isotherm, indicating that it has a microporous structure. ZSM-5 shows a steep uptake at a high relative pressure of above 0.9, which is attributed to the inter-particle voids formed by agglomeration of the nano-sized ZSM-5 crystals,¹⁸ as also be witnessed by its SEM image (Figure 3b). The MM has a combined isotherm of two parent molecular sieves, with a specific surface area and pore volume between those of SAPO-34 and ZSM-5. However, the adsorption-desorption isotherms of the SAPO-34/ZSM-5 composites (C-1 and C-2) are significantly different from that of the mechanical mixture; there is a hysteresis loop at a relative pressure above 0.4, indicative of substantial mesoporosity. The appearance of the mesopores in the composites may arise from interspaces between ZSM-5 and SAPO-34 with different framework

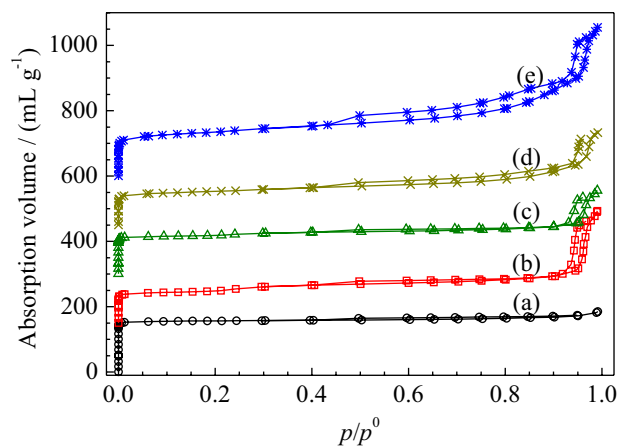


Figure 6. Nitrogen adsorption-desorption isotherms of various zeolite samples: (a) SAPO-34; (b) ZSM-5; (c) SAPO-34 and ZSM-5 MM; (d) SAPO-34/ZSM-5 composite C-1; and (e) SAPO-34/ZSM-5 composite C-2.

Table 1. Textural properties of the as-synthesized zeolite samples

Zeolite	Surface area / (m ² g ⁻¹)			Pore volume / (m ³ g ⁻¹)		
	Total	Micropore	External	Total	Micropore	Mesopore
SAPO-34	514	495	19	0.28	0.23	0.05
ZSM-5	330	278	52	0.53	0.15	0.38
MM	391	358	33	0.39	0.18	0.21
C-1	348	251	97	0.43	0.12	0.31
C-2	461	241	220	0.70	0.12	0.58

structures. With the increase of ZSM-5 content in the composite, the hysteresis loop becomes larger. Meanwhile, the mesoporous surface area and pore volume of the composite C-2 are also much higher than those of C-1, as listed in Table 1, whereas the microporous surface area and pore volume of these two composites are at the same level. As a result, it can be inferred that the increment of mesopores in the composite C-2 is mainly ascribed to the interspaces formed between ZSM-5 and SAPO-34 crystals as well as those among the small ZSM-5 crystals.

Acidic properties

NH₃-TPD profiles are displayed in Figure 7, to clarify the nature and distribution of the acid sites on the as-synthesized zeolites. Two desorption peaks corresponding to the weak and strong acid sites appear on the NH₃-TPD profiles of SAPO-34 and ZSM-5 as well as their MM. SAPO-34 has the most and strongest acid sites. Because of the high Si/Al ratio (200) and small crystal size, the acidic density of ZSM-5 synthesized in this work is relatively low. The acidic distribution of the MM is just an average of two parent zeolites. However, the acidic distribution of the SAPO-34/ZSM-5 composites is

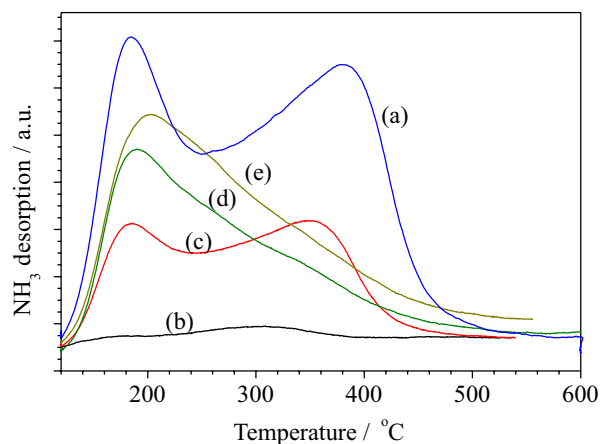


Figure 7. NH₃-TPD profiles of various zeolite samples: (a) SAPO-34; (b) ZSM-5; (c) SAPO-34 and ZSM-5 MM; (d) SAPO-34/ZSM-5 composite C-1; and (e) SAPO-34/ZSM-5 composite C-2.

Table 2. Methanol conversion and product distribution for MTH reaction over various as-synthesized zeolite samples

Zeolite	Methanol conversion / %	Selectivity / wt. %					
		Total alkanes	C ₂ =	C ₃ =	C ₄ =	Total alkenes	Aromatics
SAPO-34	99.8	3.4	48.7	37.1	8.6	96.4	0.2
ZSM-5	99.0	8.0	2.7	43.7	23.3	90.2	1.9
MM	98.0	6.7	1.6	38.7	21.9	91.6	1.7
C-1	96.8	24.6	4.9	33.8	15.9	70.7	4.7
C-2	99.0	25.6	7.5	34.3	18.0	69.0	5.4

Reactions were carried out at atmospheric pressure, 450 °C, with a methanol WHSV of 1 h⁻¹; the molar fraction of methanol in the feed is 0.2, through the dilution with nitrogen. The data were acquired after 4 h on stream.

quite different from those of the parent zeolites and their mechanical mixture; the profiles of the composites only have a desorption peak at low temperature corresponding to weak acid sites. Compared with the parent zeolites, the fraction of strong acidic sites for the SAPO-34/ZSM-5 composites is remarkably reduced. Meanwhile, Figure 7 also illustrates that the acidic quantity and strength of the composite C-2 with higher ZSM-5 content are slight higher than those of the composite C-1.

Catalytic performances

To characterize the catalytic performances of the SAPO-34/ZSM-5 composites in the MTH reaction, the conversion of methanol as a function of time on stream over various zeolites are illustrated in Figure 8; meanwhile, the methanol conversion and product distribution for MTH after reaction for 4 h are listed in Table 2. All the zeolite samples exhibit a high initial activity, with a high methanol conversion (>97%) at the initial stage. SAPO-34 deactivates very quickly, whereas ZSM-5 has the longest life time. Meanwhile, little improvement in the catalytic stability is observed for the MM of ZSM-5 and SAPO-34. However, the catalytic stability of the SAPO-34/ZSM-5 composites, especially C-2 with a SAPO-34/ZSM-5 weight ratio of 1/2, is remarkable enhanced and even close to that of ZSM-5. Obviously, the combination of ZSM-5 into SAPO-34 in the composite can improve the catalyst stability to a large extent relative to that of SAPO-34. This may be attributed to that the SAPO-34/ZSM-5 composites are provided with mesoporous structure, small crystal size, and relatively weak acidity, which is effective in promoting the product diffusion and alleviating the coke deposition.

As for the product distribution for MTH, SAPO-34 gives high selectivity to light olefins, especially to ethene, whereas ZSM-5 yields more higher olefins like propene and butene. Compared with the parent SAPO-34 and ZSM-5 zeolites as well as their mechanical mixture, however, the selectivity to total alkenes over the composites C-1 and C-2

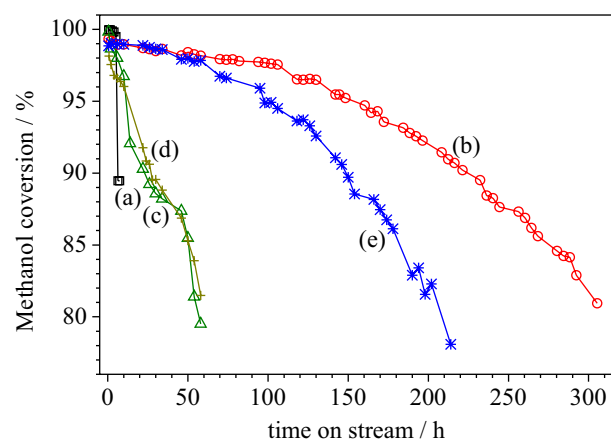


Figure 8. Methanol conversion as a function of time on stream in MTH over various zeolite samples: (a) SAPO-34; (b) ZSM-5; (c) SAPO-34 and ZSM-5 MM; (d) SAPO-34/ZSM-5 composite C-1; and (e) SAPO-34/ZSM-5 composite C-2.

is evidently reduced, whereas the selectivity to total alkanes and aromatics is enhanced, suggesting the SAPO-34/ZSM-5 composites are in favor of the formation of alkanes and aromatics. It is well known that the catalytic activity and selectivity of zeolites for MTH reaction are influenced not only by their pore dimensions but also by their acidic properties;¹⁹ the formation of light alkenes are favored on strong acid sites and narrow pores. Hence, the decrease of the selectivity to alkenes over the SAPO-34/ZSM-5 composites can be attributed to the decrease of strong acid sites and the improvement in meso-porosity.

Conclusions

By using the nano-sized ZSM-5 zeolite as seeds, SAPO-34/ZSM-5 composite was successfully synthesized. The as-synthesized SAPO-34/ZSM-5 composite takes the form of sphere-like particles with a diameter ranging from 2.3 to 4.8 μm, through the accumulation of tiny ZSM-5 and SAPO-34 crystals; a large quantity of mesopores was formed in the interspaces between ZSM-5 and SAPO-34 crystals. Meanwhile, the fraction of strong acidic sites for

the SAPO-34/ZSM-5 composites is remarkably reduced, compared with the parent zeolites and their mechanic mixture.

Owing to the proper acidity and porosity, the SAPO-34/ZSM-5 composite exhibits higher stability in MTH and favors the formation of aromatics and alkanes, compared with the parent SAPO-34 and ZSM-5 zeolites and their mechanical mixture.

Acknowledgments

The authors are grateful for the help from Prof Zhangfeng Qin in Institute of Coal Chemistry, Chinese Academy of Science in the final revision of the manuscript in English text and illustrations as well as the financial supports of the National Natural Science Foundation of China (21273264, 21273263, 21403268), and Natural Science Foundation of Shanxi Province of China (2012011005-2 and 2013021007-3).

References

1. Stöcker, M.; *Microporous Mesoporous Mater.* **1999**, *29*, 3.
2. Liu, Z.; Sun, C.; Wang, G.; Wang, Q.; Cai, G.; *Fuel Process. Technol.* **2000**, *62*, 161.
3. Yokoi, T.; Yoshioka, M.; Imai, H.; Tatsumi, T.; *Angew. Chem., Int. Ed.* **2009**, *48*, 9884.
4. Bleken, F.; Skistad, W.; Barbera, K.; Kustova, M.; Bordiga, S.; Beato, P.; Lillerud, K. P.; Svelle, S.; Olsbye, U.; *Phys. Chem. Chem. Phys.* **2011**, *13*, 2539.
5. Teketel, S.; Skistad, W.; Benard, S.; Olsbye, U.; Lillerud, K. P.; Beato, P.; Svelle, S.; *ACS Catal.* **2012**, *2*, 26.
6. Westgård Erichsen, M.; Svelle, S.; Olsbye, U.; *J. Catal.* **2013**, *298*, 94.
7. Olsbye, U.; Svelle, S.; Bjørgen, M.; Beato, P.; Janssens, T. V. W.; Joensen, F.; Bordiga, S.; Lillerud, K. P.; *Angew. Chem., Int. Ed.* **2012**, *51*, 5810.
8. Fan, Y.; Bao, X.; Lei, D.; Shi, G.; Wei, W.; Xu, J.; *Fuel* **2005**, *84*, 435.
9. Fan, Y.; Lei, D.; Shi, G.; Bao, X.; *Catal. Today* **2006**, *114*, 388.
10. Zhang, X.; Wang, J.; Zhong, J.; Liu, A.; Gao, J.; *Microporous Mesoporous Mater.* **2008**, *108*, 13.
11. Prokešová, P.; Žilková, N.; Mintova, S.; Bein, T.; Čejka, J.; *Appl. Catal., A* **2005**, *281*, 85.
12. Xue, B.; Xu, J.; Xu, C.; Wu, R.; Li, Y.; Zhang, K.; *Catal. Commun.* **2010**, *12*, 95.
13. Chae, H.-J.; Song, Y.-H.; Jeong, K.-E.; Kim, C.-U.; Jeong, S.-Y.; *J. Phys. Chem. Solids* **2010**, *71*, 600.
14. Duan, C.; Zhang, X.; Zhou, R.; Hua, Y.; Chen, J.; Zhang, L.; *Catal. Lett.* **2011**, *141*, 1821.
15. Jang, H.-G.; Min, H.-K.; Lee, J. K.; Hong, S. B.; Seo, G.; *Appl. Catal., A* **2012**, *437-438*, 120.
16. Jacobs, P. A.; Beyer, H. K.; Valyon, J.; *Zeolites* **1981**, *1*, 161.
17. Ashtekar, S.; Chilukuri, S. V. V.; Chakrabarty, D. K.; *J. Phys. Chem.* **1994**, *98*, 4878.
18. Xue, T.; Wang, Y. M.; He, M.-Y.; *Microporous Mesoporous Mater.* **2012**, *156*, 29.
19. Min, H.-K.; Park, M. B.; Hong, S. B.; *J. Catal.* **2010**, *271*, 186.

Submitted on: May 18, 2014

Published online: November 25, 2014